ACS OMEGA

http://pubs.acs.org/journal/acsodf

Article

Green Synthesis of Sulfur- and Nitrogen-Doped Carbon Quantum Dots for Determination of L-DOPA Using Fluorescence Spectroscopy and a Smartphone-Based Fluorimeter

Amir Hemmati, Hamid Emadi,* and Seyed Reza Nabavi

Cite This: *ACS Omega* 2023, 8, 20987−20999

Read Online

ACCESS | Metrics & More | Article Recommendations | Supporting Information

ABSTRACT: Sulfur- and nitrogen-doped carbon quantum dots (S,N-CQDs) were synthesized using feijoa leaves as a green precursor via a novel route. Spectroscopic and microscopic methods such as X-ray photoelectron spectroscopy, fluorescence spectroscopy, and high-resolution transmission electron microscopy were used to analyze the synthesized materials. The blue emissive S,N-CQDs were applied for qualitative and quantitative determination of levodopa (L-DOPA) in aqueous environmental and real samples. Human blood serum and urine were used as real samples with good recovery of 98.4−104.6 and 97.3−104.3%, respectively. A smartphone-based fluorimeter device was employed as a novel and user-friendly self-product device for pictorial determination of L-DOPA. Bacterial cellulose nanopaper (BC) was used as a substrate for S,N-CQDs to make an optical nanopaper-based sensor for L-DOPA determination. The S,N-CQDs demonstrated good selectivity and sensitivity. The interaction of L-DOPA with the functional groups of the S,N-CQDs via the photo-induced electron transfer (PET) mechanism quenched the fluorescence of S,N-CQDs. The PET process was studied using fluorescence lifetime decay, which confirmed the dynamic quenching of S,N-CQD fluorescence. The limit of detection (LOD) of S,N-CQDs in aqueous solution and the nanopaper-based sensor was 0.45 μM in the concentration range of 1−50 μM and 31.05 μM in the concentration range of 1−250 μM, respectively.

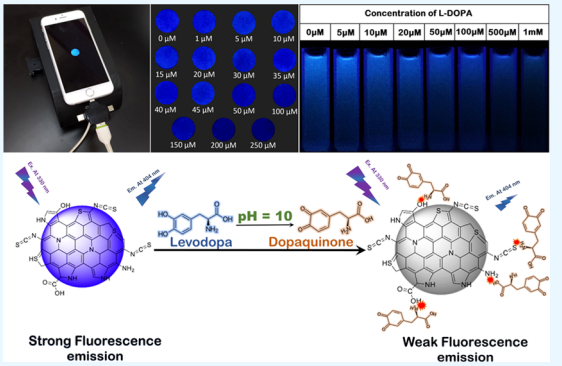

INTRODUCTION

Parkinson's illness (PI) is a neurodegenerative untidiness, and it is classified by three types of cardinal symptoms: bradykinesia, rigidity, and tremor.[1] PI is the second most universal neurodegenerative untidiness, and millions of people in the world are suffering from the effects of this disease. PI occurs due to dopaminergic neuronal loss in the substantia nigra. That will happen frequently to those over the age of 60.[2]

Typically, pharmaceutical dopamine replacement is needed to treat PI. Levodopa (L-DOPA) is the most often used medication for treating PI.[3] The "gold standard" of current PI medication therapy is L-DOPA. L-DOPA is captured by lingering dopamine neurons and converted into dopamine, which is kept and gently released into the synapse over time. Unlike dopamine, which cannot pass over the blood−brain barrier, the passage of L-DOPA into the brain is assisted by the large impartial amino acid passage system.[4,5]

L-DOPA has so many benefits for the treatment of PI. However, there are potential problems such as side effects with L-DOPA treatment including nausea, vomiting, postural hypotension, and cardiac rhythm disturbance. Sedation, vivid dreams, nightmares, and hallucinations are other side effects, mainly in aged patients. Additional psychological disorders such as disorientation, paranoia, and manic states might also occur.[6] As a result, determining L-DOPA sensitively and selectively is critical to avoiding treatment-related side effects.

Up to now, many attempts have been made for determining L-DOPA, such as electrochemical methods,[7,8] fluorescence methods,[9,10] capillary electrophoresis,[11] high-performance liquid chromatography (HPLC),[12] and spectrophotometry.[13] However, these methods which are not costly, have a low limit of detection (LOD) and a quick measuring duration, and do not require expert technicians.

Fluorescent nanoparticles have various advantages as fluorescent sensors. Fluorescent materials, for example, have high sensitivity and reasonable specificity.[14] This sensitivity can be 1000 times higher than spectrophotometric methods.[15] Moreover, fluorescent materials can detect single molecules, resulting in high detection sensitivity.[16] Furthermore, fluorescence spectroscopy is a suitable choice for sensing applications due to its ease of use.[17] On the other hand, regular

Received: March 16, 2023
Accepted: May 24, 2023
Published: May 31, 2023

ACS Publications

© 2023 The Authors. Published by American Chemical Society

organic dyes and other common fluorescent materials have disadvantages, like high LOD or low quantum yields. But, progress in nanotechnology caused the development of fluorescent nanomaterials with unique optical properties and narrow size distribution, which opened a new way to prepare fluorescent sensors based on nanomaterials.[18]

Many materials can be used as fluorescent probes. Carbon quantum dots (CQDs) are an excellent choice among them due to their various advantages like non-toxicity, high quantum yield,[19] exceptional photostability, ease of preparation, and good stability. As a result, they are ideal candidates for sensing applications.[20] Also, CQDs can determine non-fluorescent drugs by fluorescence quenching, which is a great advantage for sensing drugs.[21] CQDs have been utilized in numerous fields, such as nanosensing,[22] bioimaging,[23] catalysis,[24] and optoelectronic[25] uses. Low-cost production of sensors is considered an advantage. In this way, CQDs can be produced from low-cost precursors, including citric acid as noncomplex organic molecules or more heterogeneous precursors such as orange juice, rice, leaves, ashes, or even waste.[26,27] This means they can be synthesized almost from every organic material around us.

Feijoa sellowiana is a monotypic type of the Myrtaceae family which is usually identified as the pineapple guava or guavasteen and is nearly associated with guava, *Psidium guajava L.* The feijoa is a perennial plant that emerges from the uplands of north-eastern and eastern areas of South America. It has been widely distributed due to its easy compatibility in subtropical regions. Recently, it is widely cultured in many countries, including Iran.[28,29] It seems that feijoa leaves are a very suitable material to synthesize CQDs because they are inexpensive, easy to find, and biocompatible.

There are numerous ways for synthesizing CQDs, such as supercritical or subcritical water method,[30,31] arc-discharge, laser ablation, electrooxidation, thermal oxidation, pyrolysis with microwave,[32] ultrasonic synthesis, thermal pyrolysis, and hydrothermal synthesis.[33] Microwave-assisted preparation of CQDs offers several advantages over other bottom−up methods. The microwave approach needs a shorter reaction time in comparison with conventional methods like the hydrothermal method. Furthermore, microwave heating systems are more efficient and produce fewer side reactions, as well as fewer by-products. Consequently, this method can reduce the number of purification steps.[34] In convection or conduction methods, heat transfer is not uniform, which results in the formation of by-products or incomplete reactions. Also, these methods need a longer reaction time to reach the desired temperature. Unlike conventional heating methods, microwave radiation heats the sample molecules at the moment and accelerates the reaction.[35]

The fluorescence intensity of CQDs is increased by nitrogen and sulfur doping.[36,37] S,N-CQDs are good candidates for the determination of L-DOPA due to the presence of some functional groups like −SCN, −OH, and $-CONH_2$ on the surface of S,N-CQDs.[38] S,N-CQDs are among the most distinguished doped CQDs because nitrogen has an atomic radius comparable to carbon. Also, sulfur and carbon have similar electronegativity.[39] It is believed that S,N-CQDs can interact with L-DOPA, leading to fluorescence quenching of the S,N-CQDs.[40] Up to now, researchers have reported the interaction of dopamine, L-DOPA, and metal ions with functional groups of the S,N-CQDs.[41,42] These interactions may result in static or dynamic quenching and improve target analyte determination.

Smartphones have been used in various applications in recent years, owing to the advent of high-resolution cameras and the computing capability of smartphones, which made them suitable for generating smartphone-based devices in sensing applications.[43] The analytical methods for sensing applications have many difficulties, including expensive apparatus, bulky systems, and devices with a high degree of complexity.[44] Moreover, smartphone-based devices are portable, affordable, easy to use, and sensitive.[45] According to these conditions, various devices have been developed, such as smartphone-based devices that use fluorescence nanopapers to detect biological and chemical materials. Bacterial cellulose nanopaper (BC) is a suitable substrate for CQDs because they can be supportive, biocompatible, biodegradable, optically transparent, thermally stable, flexible, hydrophilic, and highly porous materials, and are able to undergo wide ranges of chemical modifications with an extraordinary surface area.[46,47] Usually, BC originated from carbon sources like glucose by nonpathogenic bacteria such as *Gluconacetobacter xylinus*. The flexibility, cheap cost, and biocompatibility of these cellulosic materials make them an ideal platform for sensing technologies.[48]

Red, green, and blue (RGB) detection methods are useful for evaluating data obtained from fluorimeter devices and would be a suitable technique to determine target analytes. RGB-based sensors can be monitored by bare eyes and smartphone cameras, which is an advantage for producing user-friendly devices.[49] Fabrication of such a device can help to determine L-DOPA using S,N-CQDs deposited on BC (S,N-CQDs-BC). S,N-CQDs-BC shows strong blue fluorescence under 365 nm UV light emitting diode (LED) light, and the signals can be analyzed using a smartphone as a fast and sensitive sensing system. RGB detector programs for smartphones, such as the Color Detector app, can analyze RGB data. In the current study, for the first time, CQDs with −SCN functional groups were synthesized via a green and fast method. A self-made smartphone-based fluorimeter device was utilized to determine L-DOPA by the synthesized S,N-CQDs. This platform is a new device that can be connected to any smartphone, making it a user-friendly platform for determining chemical and biological materials.

EXPERIMENTAL SECTION

Materials. The chemicals were not purified in any way, which were analytical grade. Ethanol, L-glutamine, L-cysteine, ascorbic acid, urea, citric acid, NaCl, $CaCl_2$, thiourea, sodium carbonate, sodium bicarbonate, disodium hydrogen phosphate, and potassium dihydrogen phosphate were purchased from Merck KG, Darmstadt, Germany. 3,4-Dihydroxyphenylalanine (L-DOPA) and quinine sulfate were purchased from Sigma Aldrich. *F. sellowiana* leaves were collected from the University of Mazandaran campus. Before use, the leaves were washed and dried for the elimination of impurities. For all experiments, double distilled water was used.

Instruments. Molecular vibration data were collected with a Fourier transform infrared (FT-IR) spectrometer (BRUKER Tensor 27). The Raman spectrum was recorded on a Raman spectrometer (Teksan Takram-532 nm laser excitation). The elemental composition and contents were measured by X-ray photoelectron spectroscopy (XPS) (SPECS UHV analysis system). High-resolution transmission electron microscopy

https://doi.org/10.1021/acsomega.3c01795
ACS Omega 2023, 8, 20987−20999

Scheme 1. Graphical Representation of the Current Study

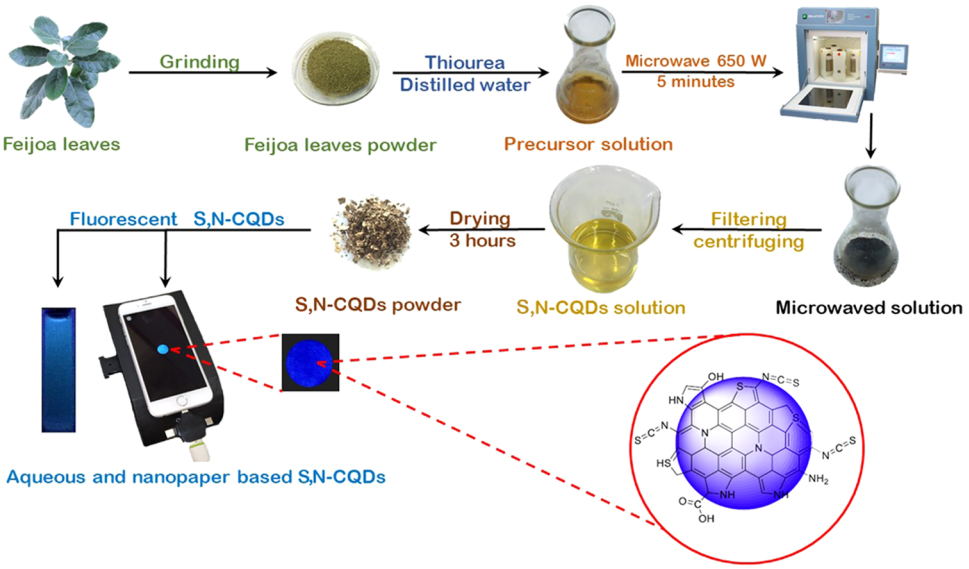

(HR-TEM) was accompanied by the use of an FEI Tecnai G^2 F20 SuperTwin TEM (accelerating voltage: 200 kV). Microstructures and dispersion of S,N-CQDs were observed by field emission scanning electron microscopy (FE-SEM), (MIRA 3-XMU) equipped with energy-dispersive X-ray spectroscopy (EDS), (TESCAN MIRA II). X-ray diffraction (XRD) analysis was performed on an X-ray powder diffractometer (Philips PW1730). The specific Brunauer−Emmet−Teller (BET) surface area was evaluated by nitrogen adsorption at 77 K (Bell Belsorb-mini II). UV−vis absorption and fluorescence spectra were scanned using a UV−visible spectrophotometer (Jasco V-750) and fluorescence spectrophotometer (Jasco FP-8300), respectively. The fluorescence lifetime decay of samples was studied on a steady state and a transient state fluorescence spectrometer (Edinburgh Instruments ex-demo equipment f900 spectrophotometer). MILESTONE MICROSYNTH was utilized to synthesize S,N-CQDs via microwave-assisted synthesis.

Synthesis of S,N-CQDs. Microwave-assisted pyrolysis was used to synthesize the S,N-CQDs. As a green material, feijoa leaves were employed as a precursor in the synthesis process. Synthesis parameters were optimized as presented in Table S1. In a typical optimized synthesis procedure, feijoa leaves were washed with distilled water and dehydrated at 50 °C overnight. S,N-CQDs were synthesized using dry powder of feijoa leaves. To extract the feijoa leaves, 1 g of feijoa leaves powder was added to 10 mL of double distilled water, and the mixture was stirred for 1 h at room temperature. Afterward, the solution was filtered to separate solid particles. To synthesize S,N-CQDs, 0.5 g of thiourea was dissolved in 10 mL of double distilled water and the solution was added to extract the solution. The resulting solution was then microwaved for 5 min at a power of 650 W. The black solid was collected and mixed with 15 mL of double distilled water and sonicated for 10 min. The obtained mixture was centrifuged at 8000 rpm for 10 min, and the yellowish solution was collected. A 0.22 μm sterile syringe filter was used to filter the yellowish solution to remove aggregated and bulky S,N-CQDs and dried at 50 °C for 3 h and the solid S,N-CQDs were collected. The solid S,N-CQDs were washed with ethanol and double distilled water to remove unreacted organic materials. Finally, the pure brownish S,N-CQDs powder was collected and used for the next step. The synthesis process is summarized graphically in Scheme 1.

Calculation of the Quantum Yield (QY). The QY of the synthesized S,N-CQDs was measured using quinine sulfate (in 0.1 M H_2SO_4 as a solvent, QY = 54%) as a reference compound. The desired solution of the reference and S,N-CQDs was prepared in 0.1 M H_2SO_4 and double distilled water, respectively. The UV−vis absorption of both solutions was measured. Then, the fluorescence spectra of both solutions were evaluated at the excitation wavelength of 330 nm, and the absorbance of both solutions was measured at the 330 nm wavelength from the UV−vis absorption spectrum of solutions. Afterward, the integrated fluorescence intensity (area under the spectrum) of both solutions was measured, and the collected data were used to calculate QY.

L-DOPA Determination by Fluorescence. The determination was done at room temperature and in a carbonate−bicarbonate buffer (0.1 M, pH 10). A 1000 ppm S,N-CQD stock solution in double distilled water was made. The stock solution of S,N-CQDs was diluted to 200 ppm S,N-CQDs for fluorescence analysis with carbonate−bicarbonate buffer. Different concentrations of L-DOPA were prepared in double distilled water. In this regard, 1.5 mL of the as-prepared solution of S,N-CQDs was mixed with 1.5 mL of different concentrations of L-DOPA solution (1−1000 μM). The ultimate volume (3 mL) of the mixture was incubated for 5 min. Then, the fluorescence spectra of the solution were recorded at an excitation wavelength of 330 nm and an emission wavelength of 404 nm.

Selectivity Study and Real Sample Analysis. To investigate the selectivity of S,N-CQDs, different samples, such as L-glutamine, ascorbic acid, L-cysteine, urea, citric acid, NaCl, and $CaCl_2$, were used. 1.5 mL of the same concentration of each sample was added to 1.5 mL of 200 ppm of S,N-CQDs in carbonate−bicarbonate buffer (0.1 M, pH 10), and incubated for 5 min, and fluorescence spectra were recorded at an excitation wavelength of 330 nm and an emission wavelength of 404 nm.

In addition, real sample analysis was conducted on human blood serum and urine samples. The human blood serum and urine samples were obtained from a healthy human. The

https://doi.org/10.1021/acsomega.3c01795
ACS Omega 2023, 8, 20987−20999

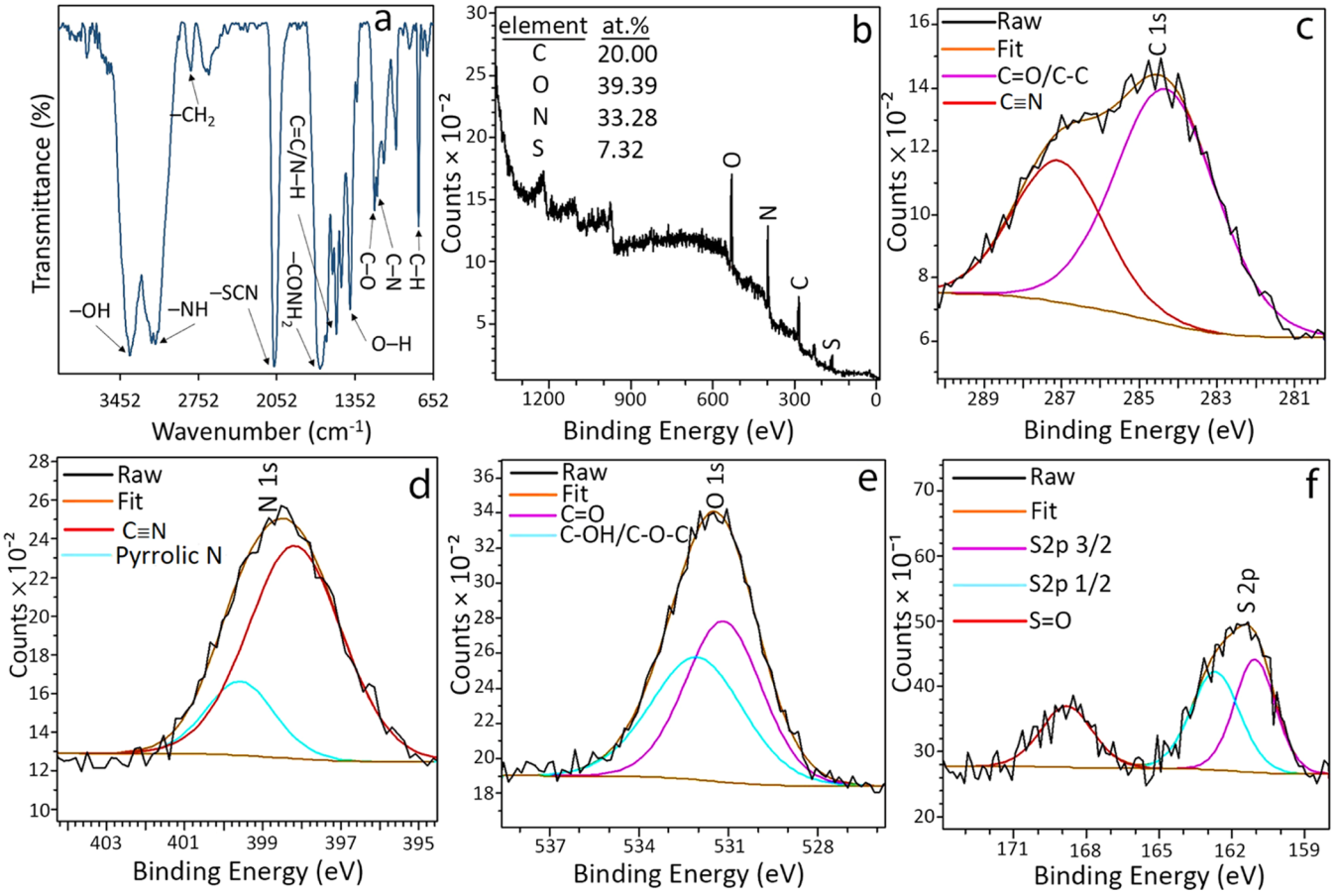

Figure 1. (a) FT-IR spectra of S,N-CQDs and (b) full XPS survey spectrum, (c) C 1s, (d) N 1s, (e) O 1s, and (f) S 2p of S,N-CQDs.

human blood serum and urine samples were filtered using a 0.22 μm sterile syringe filter and centrifuged at 8000 rpm for 10 minutes to rectify bulky particles. Afterward, a phosphate buffer solution was added to the serum and urine samples to dilute them 50 times.[50,51] Briefly, three concentrations of L-DOPA (5, 25, and 50 μM) were prepared by the human blood serum and urine samples. 1.5 mL of these solutions were mixed with 1.5 mL of 200 ppm of S,N-CQDs in carbonate–bicarbonate buffer (0.1 M, pH 10) and incubated for 5 min and fluorescence spectra were recorded at an excitation wavelength of 330 nm and an emission wavelength of 404 nm.

Preparation of Smartphone-Based Fluorimeter Device. The framework of the device was prepared by 3D printing (Figure S1). This framework contains a 365 nm UV LED light, UV pass filter, portable S,N-CQDs-BC holder, USB cable, USB OTG, and a slot for smartphone. The LED is powered by a smartphone battery. The S,N-CQDs-BC is made by adding one drop of S,N-CQDs solution on the BC and drying of S,N-CQDs-BC at room temperature. For the determination of L-DOPA, one drop of different concentrations of L-DOPA was added to S,N-CQDs-BC, and the fluorescence was pictured by the prepared smartphone-based fluorimeter device.

RESULTS AND DISCUSSION

Material Characterization. The functional groups of the S,N-CQDs were categorized by FT-IR spectroscopy (Figure 1a). At ∼3360 and ∼3170 cm^{-1}, the bands with broad vibration correspond to the O–H and N–H stretching vibrations, respectively. The peak at ∼1660 cm^{-1} is endorsed by the stretching vibration of the $-CONH_2$ group. The bending vibrations of C=C/N–H and O–H are ascribed to ∼1530 and ∼1395 cm^{-1}, respectively. The C–O and C–N stretching bands are observed at ∼1178 and ∼1155 cm^{-1}, respectively. The peaks at ∼2815 and ∼784 cm^{-1} correspond to C–H stretching and bending vibrations, respectively. The sharp peak at ∼2070 cm^{-1} is attributed to the –SCN group. The S–H stretching vibration is seen at around 2500 cm^{-1} which is not a sharp peak due to the breaking of the S–H bond and conversion to –SCN groups.[38,52−54] The FT-IR analysis results confirm the presence of the $-CONH_2$, –OH, $-NH_2$, and –SCN groups on the S,N-CQDs, which may originate from the composition of the feijoa leaves as the precursor of S,N-CQDs.[38]

The composition of elements of the S,N-CQDs was categorized by the XPS method, EDS, and elemental mapping analysis (Figure S2). Figure 1b displays the XPS spectrum of S,N-CQDs in complete-scan analysis, which confirms the existence of C, N, O, and S elements in the synthesized S,N-CQDs. The peaks of O 1s at 532, N 1s at 399, C 1s at 285, and S 2p at 162 eV can be seen in Figure 1b. There are two main peaks in C 1s XPS spectrum (Figure 1c) which are attributed to the sp^2 and sp^3 hybridized carbon atoms. The peak at ∼284.31 eV corresponds to C–C/C=C, while the peak at ∼287.1 eV belongs to C≡N. In the N 1s XPS spectrum (Figure 1d), two main peaks are found. The peak at ∼398.2 eV represents the –C≡N groups existing in S,N-CQDs, while the other peak at ∼399.6 eV originated from the pyrrolic and

https://doi.org/10.1021/acsomega.3c01795
ACS Omega 2023, 8, 20987−20999

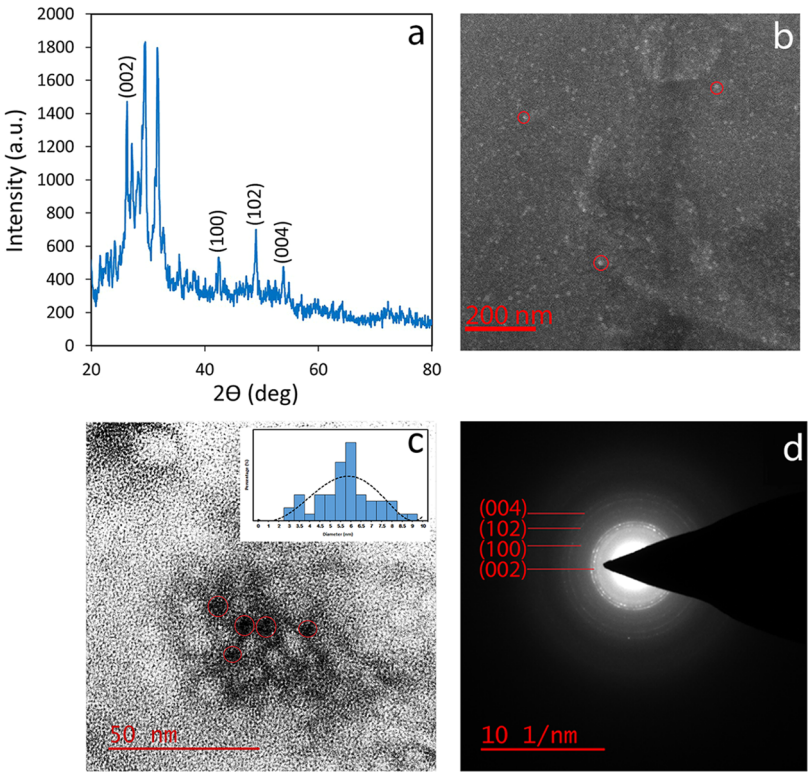

Figure 2. (a) XRD pattern, (b) FE-SEM image, (c) HR-TEM image, histogram of size distribution shown as inset, and (d) SAED pattern of S,N-CQDs.

graphitic N atoms.[52] The peaks at ∼531.2 and ∼532.0 eV (Figure 1e) confirm the presence of C═O and C−OH/C−O−C groups, respectively.[55] The ∼161.1 and ∼162.7 eV peaks in the XPS spectrum of S 2p (Figure 1f) correspond to S $2p_{3/2}$ and S $2p_{1/2}$, respectively. This observation can be attributed to the C−S−C covalent bond in the structures like thiophene due to the spin-orbit splitting. Also, the peak at ∼168.8 eV represents the −C−SO_x−C− sulfone bridges.[52] Based on the XPS results, the atomic ratio of S/C, O/C, and N/C are estimated at 0.37, 1.97, and 1.66, respectively. The results indicate that the S,N-CQDs are oxygen and nitrogen-rich on the surface.[56,57] The existence of hydrophilic groups on the S,N-CQDs makes it more dispersible in an aqueous solution which is suitable for sensing purposes.

The crystallinity and morphology of S,N-CQDs were characterized by XRD, HR-TEM, FE-SEM, and SAED patterns. X-ray diffraction (XRD) analysis of S,N-CQDs (Figure 2a) was used for phase identification of S,N-CQDs. The diffraction peak at $2\theta = 26°$ corresponds to the graphitic-like carbons. The peaks at $2\theta = 42.5$ and 49° correspond to the (100) and (102) planes, respectively, which have arisen from the in-plane diffraction of graphitic-like organized S,N-CQDs. Also, Raman spectra (Figure S3) indicated the graphitization of S,N-CQDs because the intensity of the G to D band is greater than 1.[58] The (004) plane at $2\theta = 54°$ is the typical peak for the graphitic-like structure materials. This XRD was matched with JCDPS card No. 75-1621.[59] Also, the lattice spacings of the (002), (100), (102), and (004) planes are 0.33, 0.21, 0.18, and 0.169 nm, respectively. Due to the use of a green method for synthesizing S,N-CQDs, some extra peaks are observed in the XRD pattern, which can be attributed to the incomplete reaction and residual compounds from the extraction of feijoa leaves.[60−62] Feijoa leaf is a source of mineral elements such as calcium, potassium, sodium, and sulfur.[63] Therefore, some of these elements may remain in the final product. In this regard, the peaks at around 29 and 32° can be assigned to the calcium-based substances such as $Ca(OH)_2$.[64] Figure 2b shows the FE-SEM of S,N-CQDs, indicating no aggregation and small size of the S,N-CQDs.

Figure 2c displays the HR-TEM image of the S,N-CQDs. The average diameter of S,N-CQDs is 6 nm, which is an acceptable size for CQDs. Also, HR-TEM image indicates that S,N-CQDs have a spherical shape and narrow size distribution. According to Figure 2d, the SAED pattern confirms the polycrystalline nature of the S,N-CQDs due to the sporadic rings. The lattice spacing of 0.33, 0.21, 0.18, and 0.169 nm for S,N-CQDs obtained by the XRD, were in good agreement with data calculated by the SAED pattern (Table S2).[65]

The lattice spacing of 0.21 nm is related to the (100) planes in the direction of the [1010] planes (Figure 3a). Also, in most of the CQDs, crystal lattice spacing is in the range of 0.18−0.24 nm for graphitic in-plane and 0.32 nm for graphitic interlayer spacing, which is indicated by the (002) facet of graphite (Figure 3b). Also, the FFT pattern of the (100) planes (Figure 3c) shows that they have a hexagonal structure in the [0001] direction, and Figure 3d shows the FFT pattern of S,N-CQDs for the (002) planes, demonstrating that S,N-CQDs have a graphitic framework.[66−71]

Figure S4a shows the S,N-CQDs N_2 physisorption analysis in liquid nitrogen at 77 K. The resultant adsorption−desorption isotherm of the S,N-CQDs is categorized as a type-I/IV isotherm corresponding to S,N-CQDs with microporous and mesoporous structures. The saturation vapor pressure and adsorption temperature were adjusted to 110.88 kPa and 77 K respectively for the experiment. The surface area of the S,N-CQDs was calculated to be 178.38 m^2/g using the

https://doi.org/10.1021/acsomega.3c01795
ACS Omega 2023, 8, 20987−20999

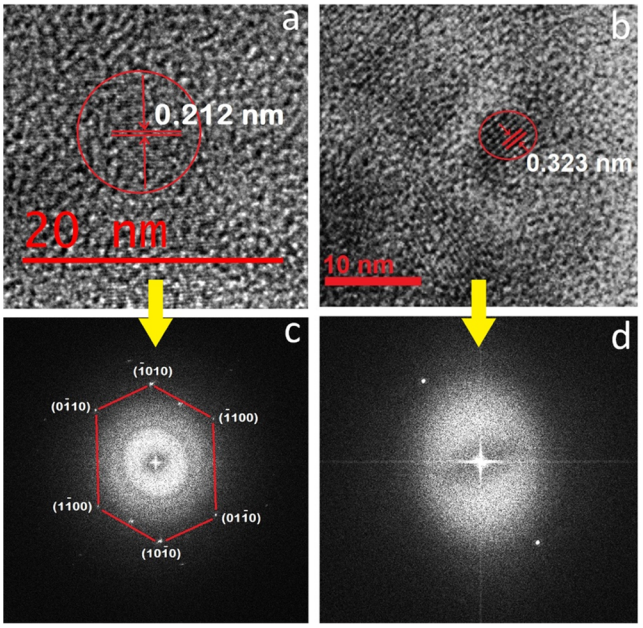

Figure 3. *d*-Spacing of S,N-CQDs with lattice spacings of (a) 0.212 and (b) 0.323 nm. (c) FFT image of S,N-CQDs for (100) planes and (d) FFT image of S,N-CQDs for the (002) planes.

Brunauer–Emmett–Teller (BET) plot (Figure S4b). Furthermore, the mean pore diameter was found to be in the 4.15 nm range by the linear fit curves. The pore size volume of the S,N-CQDs was calculated to be 0.1851 cm^3/g using the BET plot. The results have proven the micro/mesoporous nature of the S,N-CQDs, which may be used to detect analytes to a great extent.[72]

Optical Properties of S,N-CQDs. Figure 4a shows the fluorescence emission spectra of the S,N-CQDs at an excitation wavelength from 250 to 450 nm. It turned out that the intensity of fluorescence emission peaks of S,N-CQDs shifted with changes in excitation wavelength due to the presence of different functional groups on the S,N-CQDs. These functional groups are considered the excitation energy trappers, which lead to defects in the S,N-CQDs.[55] However, the differences in fluorescence emission are attributed to the surface of S,N-CQDs and more functional groups on S,N-CQDs. Also, other factors like size, surface passivation, the existence of other emissive components, and the presence of heteroatoms can affect this phenomenon.[67,73] The maximum intensity for the emission spectra was observed at 404 nm, while the excitation wavelength was 330 nm.

Figure 4b displays the fluorescence emission, excitation and UV–vis spectra of the aqueous solution of synthesized S,N-CQDs. The peak at around 290 nm in the UV–vis spectrum is attributed to the absorption of an aromatic π structure, which is related to the polycyclic aromatic hydrocarbons.[74] The strong peak at 404 nm of the fluorescence emission, which is excited at 330 nm, denoted that the synthesized S,N-CQDs have a strong blue fluorescence emission. Also, the inset shows that the synthesized S,N-CQDs have a strong blue fluorescence (right) under UV light at an excitation of 365 nm.

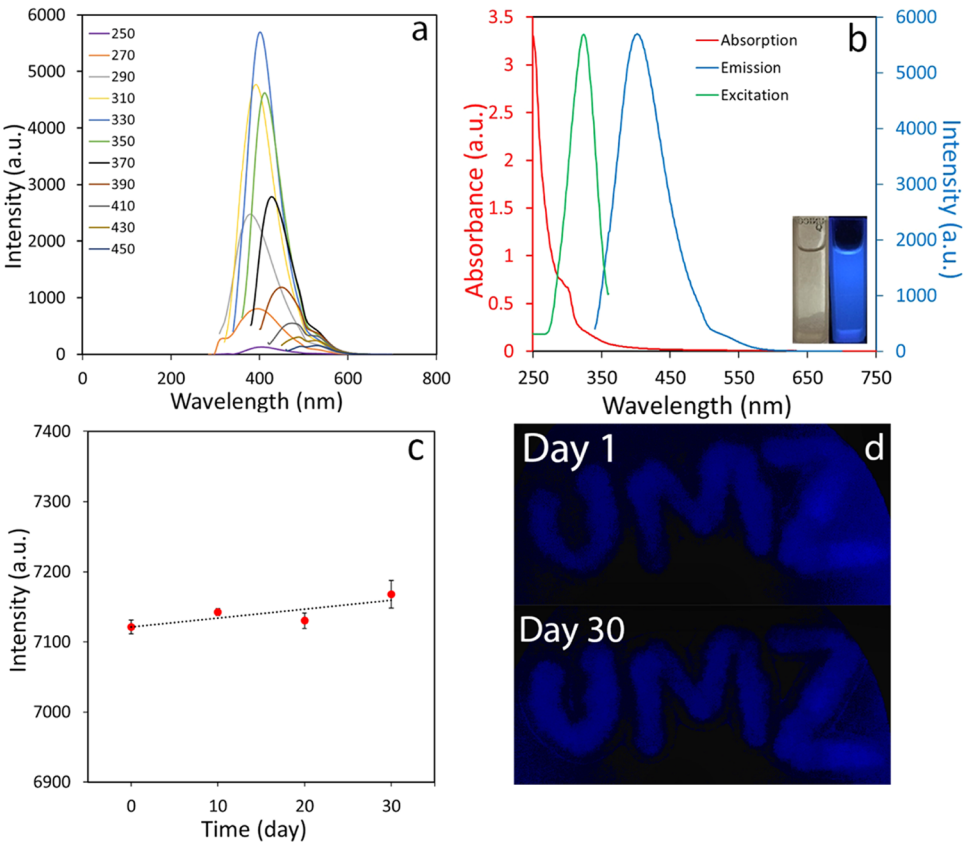

Figure 4. (a) Fluorescence emission spectra of S,N-CQDs at different excitation wavelengths from 250 to 450 nm in 10 nm increments, (b) PL emission spectra with excitation wavelengths and UV–vis absorption of the aqueous synthesized S,N-CQDs, (inset: S,N-CQD solution in daylight and under 365 nm UV light), (c) stability of S,N-CQDs from 1 to 30 days, and (d) visual stability of S,N-CQD ink from 1 to 30 days.

https://doi.org/10.1021/acsomega.3c01795
ACS Omega 2023, 8, 20987–20999

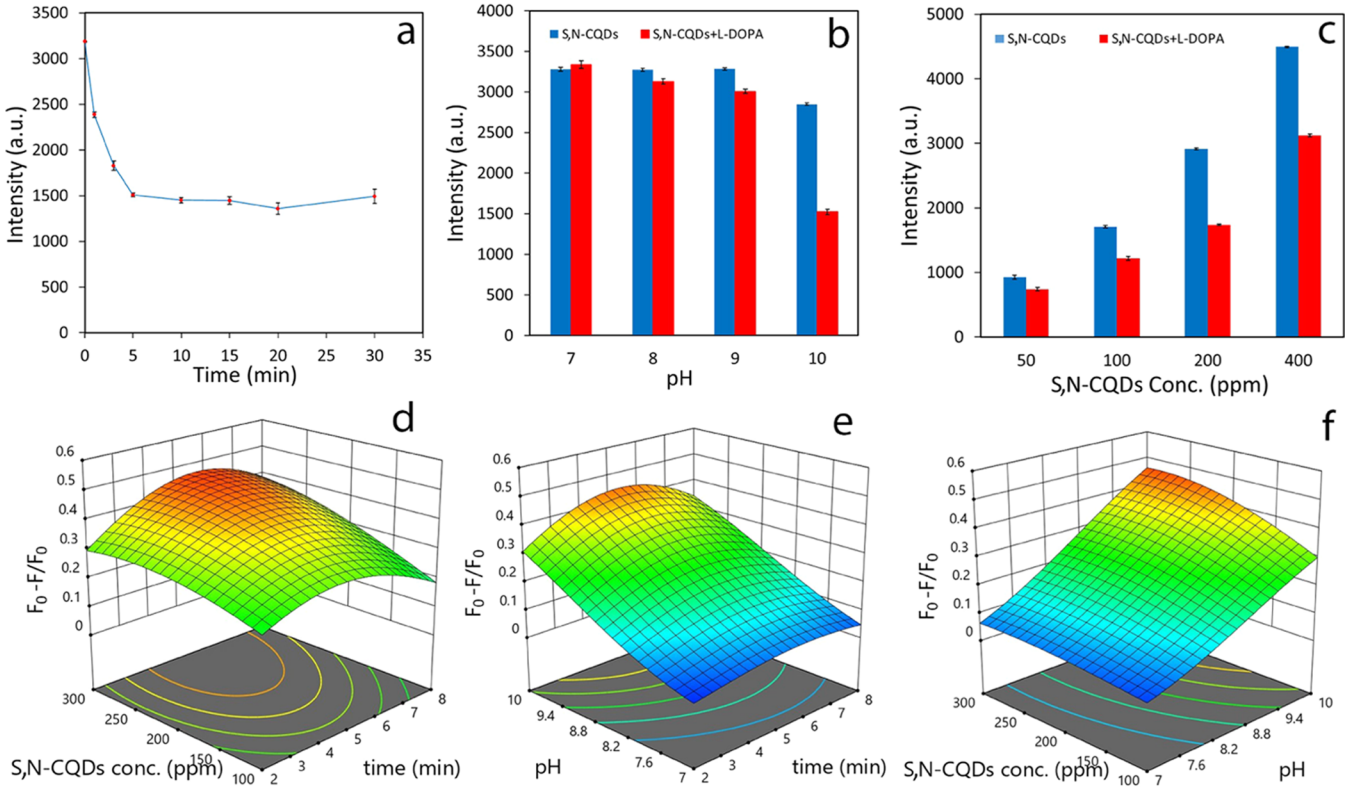

Figure 5. Optimization of (a) time, (b) pH, and (c) S,N-CQD concentration for the determination of L-DOPA. Response surfaces plot obtained based on the quenching of S,N-CQDs against the combined effect of (d) S,N-CQDs concentration and time, (e) pH and time, and (f) S,N-CQD concentration and pH.

To assess the fluorescence and optical characteristics of S,N-CQDs further, QY was calculated by eq 1

$$\Phi_s = \Phi_r \times \frac{A_r}{A_s} \times \frac{I_s}{I_r} \times \left(\frac{\eta_s}{\eta_r}\right)^2 \quad (1)$$

Φ_s and Φ_r are the quantum yield of the sample (S,N-CQDs) and reference (quinine sulfate), respectively. A_r and A_s are the absorptions at the excitation wavelength for the reference and sample, respectively. The absorption must be under 0.1 for the 1 cm × 1 cm cuvette to prevent the self-absorption of solutions. According to the experiment, 10^{-5} M quinine sulfate is suitable for this experiment. The excitation wavelength for quinine sulfate can be 260−360 nm. Beyond this excitation, the spectrum shifts to lower energy. η_r and η_s are the refractive indexes of reference and sample, respectively, which are ≈1.33 for double distilled water and 0.1 M H_2SO_4. I_s and I_r are the integrated fluorescence intensity (area under the spectrum) of the sample and reference, respectively.[75,76] The QY of S,N-CQDs was calculated (Table S3) at optimum conditions when excited at 330 nm wavelength to be 5.9% with the quinine sulfate reference (54%).

The synthesized S,N-CQDs were examined for photostability (Figure 4c) at room temperature and in a dark place from 1 to 30 days. The intensity of the fluorescence spectra of the as-synthesized S,N-CQDs (fresh S,N-CQDs) was measured and compared with incubated S,N-CQDs after 10, 20, and 30 days in the explained conditions. The results showed that the fluorescence intensity of the S,N-CQDs did not significantly change after 30 days and it just changed by less than 0.7%. Also, the photostability of S,N-CQDs was investigated by visual testing (Figure 4d) on the first day and thirtieth day by taking pictures from S,N-CQDs on filter paper, which visually confirmed the photostability of S,N-CQDs even after 30 days. These findings reveal that the S,N-CQDs have great potency in the actual sensing application and commercial purpose.

Optimization of Conditions for Determination of L-DOPA. Various parameters like pH, time, and concentration of S,N-CQDs have a significant effect on the fluorescence quenching of the S,N-CQDs. To reach a fast response for the determination of analytes by a sensor, which is critical for sensor fabrication, different parameters were optimized. Figure 5a displays the impact of time on the fluorescence quenching of the S,N-CQDs. As can be seen, after 5 min, the fluorescence quenching of the sensor was not changed significantly. So, the optimized response time was set at 5 min. The impact of pH in the range from 7 to 10 was studied. In the alkaline environment, L-DOPA changes to dopaquinone, which can interact with S,N-CQDs as a quencher.[77] In the pH range of 7−9, no remarkable fluorescence quenching of S,N-CQDs was observed. When the pH was 10, the fluorescence of S,N-CQDs quenched considerably, which could be helpful in determining L-DOPA (Figure 5b). Also, L-DOPA was incubated in different concentrations of S,N-CQDs. The results showed that at the concentration of 200 ppm of S,N-CQDs, maximum fluorescence quenching was obtained, and the quenching was not changed significantly (Figure 5c).

The relationships between the independent factors and quenching of S,N-CQDs were evaluated using central composite design (CCD) as a suitable experiment design method. The experimental results were obtained via 17 runs of

https://doi.org/10.1021/acsomega.3c01795
ACS Omega 2023, 8, 20987−20999

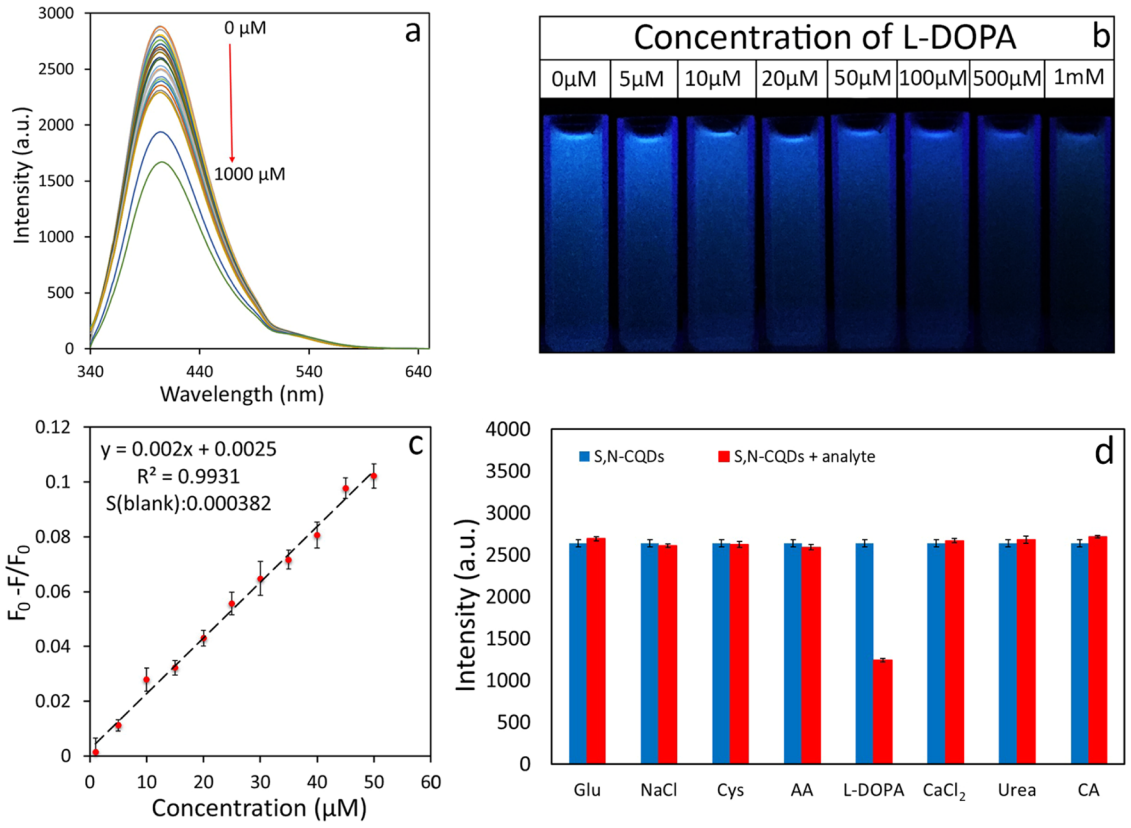

Figure 6. (a) Quenching of the fluorescence spectra of S,N-CQDs upon the addition of L-DOPA, (b) fluorescence quenching photo of S,N-CQDs under 365 nm UV light, (c) plotting the $F_0 - F/F_0$ ratio vs concentration of 1−50 μM L-DOPA, and (d) fluorescence quenching of S,N-CQDs upon the addition of different analytes.

the CCD design. The software selected the quadratic model as the recommended model. ANOVA (Table S4) was applied for the valuation of the quality and significance of the CCD design. The values of p and f were <0.001 and 347.61, respectively. These values indicated that the model was significant. Also, the p-value of the lack-of-fit is 0.6186, demonstrating that it is not significant and has good predictability.[78] The value of determination coefficient R^2 = 0.9978 (Table S5) indicates excellent fitting, and the value of adjusted R^2 (0.9949), which is a high value, indicates the significance of the CCD model. The 3D surface plot indicates the response of $F_0 - F/F_0$ (F_0 is the fluorescence intensity of S,N-CQDs before the addition of L-DOPA and F is the fluorescence intensity of S,N-CQDs after the addition of L-DOPA) on the Z-axis with every two other factors. In each plot, one of the factors is constant at its center point value (coded level: 0). The effect of both S,N-CQD concentration and time factors on the quenching of S,N-CQDs is presented in Figure 5d. The best response was found in the range of 200−300 ppm of S,N-CQDs for 4−6 min of incubation of the sample. Furthermore, the effect of pH and time on the response is shown in Figure 5e. When the pH is set in the range of 9.4−10 for 4−6 min of incubation of the sample, the response is at the highest value, which is due to the oxidation of L-DOPA under alkaline conditions. The effect of S,N-CQD concentration and pH (Figure 5f) on the quenching of S,N-CQDs indicates that in the concentration range of 200−300 ppm and pH range of 9.4−10, the best response is observed. Finally, the 3D surfaces plot of the model shows that all three factors have a significant effect on the quenching of S,N-CQDs.

3D surface plot of the model confirmed that the acceptable conditions for determining L-DOPA were achievable in 5 min of incubation, pH of 10 and 200 ppm concentration of S,N-CQDs.

Investigation of Fluorescence Quenching and Selectivity of S,N-CQDs. To investigate the sensitivity of the S,N-CQDs, various concentrations of L-DOPA (0−1000 μM) were added to an appropriate volume of S,N-CQD solution, and the fluorescence spectra of the S,N-CQDs were measured at an excitation wavelength of 330 nm and optimized conditions (Figure 6a). The results indicate that increasing the concentration of L-DOPA leads to more quenching of the S,N-CQDs fluorescence. Also, this fluorescence quenching trend was observed with bare eyes under the 365 nm UV light (Figure 6b). In various concentrations of L-DOPA, the fluorescence intensity of the S,N-CQDs at an emission wavelength of 404 nm was reduced by ca. 42% at the L-DOPA concentration of 1000 μM. These results indicate that the fluorescence intensity of S,N-CQDs is affected by the concentration of L-DOPA. Also, the linear correlation curve (y = 0.002x + 0.0025, R^2 = 0.9931) of the S,N-CQDs in L-DOPA concentrations range of 1−50 μM is presented in Figure 6c. Quantitative determination of L-DOPA showed that the LOD for the S,N-CQD sensor was 0.45 μM. Figure S5 shows the absorption spectra of S,N-CQDs, S,N-CQDs + L-DOPA, and L-DOPA. No absorption band was observed for L-DOPA, so the quenching of S,N-CQDs with L-DOPA was not due to an inner filter effect. Also, no blue-shift or red-shift was observed in S,N-CQDs before and after the addition of L-DOPA. These results indicated that the quenching of S,N-CQDs might be

https://doi.org/10.1021/acsomega.3c01795
ACS Omega 2023, 8, 20987−20999

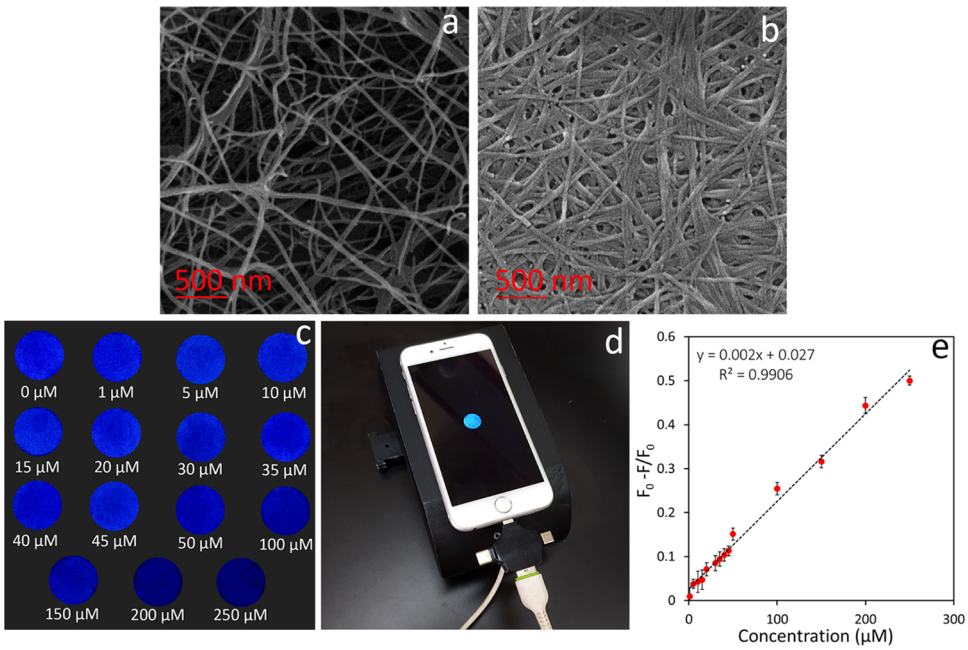

Figure 7. FE-SEM images of BC nanopaper, (a) before imprinting of S,N-CQDs, (b) after imprinting of S,N-CQDs, (c) S,N-CQDs-BC nanopaper after the addition of different concentrations of L-DOPA, (d) the fabricated device for determination of L-DOPA and (e) linear response of the S,N-CQDs-BC tape.

Scheme 2. Schematic Fluorescence Quenching Process of S,N-CQDs

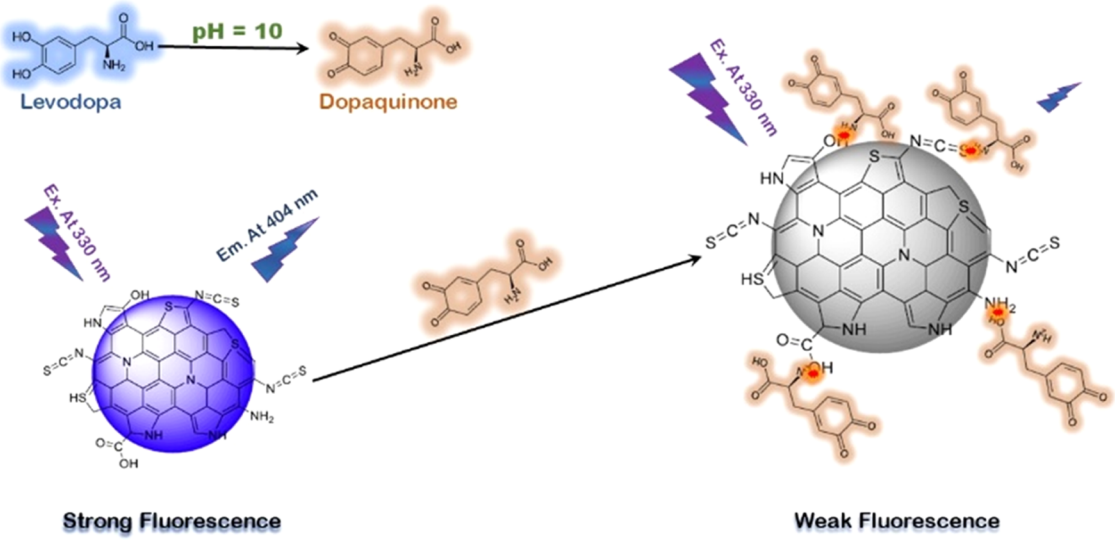

due to the molecular interaction of L-DOPA and S,N-CQDs.[79] The LOD and incubation time obtained for L-DOPA sensing were compared with similar works as shown in Table S6. It shows that current results are comparable to similar works. But, the main advantages of this study are its ease of operation and lower sensing time.

To investigate the selectivity of S,N-CQDs, different analytes such as L-glutamine, L-cysteine, ascorbic acid, urea, citric acid, NaCl, and $CaCl_2$ were added to the S,N-CQD solution with similar procedure for the addition of L-DOPA to the S,N-CQD sample. The results (Figure 6d) confirmed that the other analytes did not significantly affect the fluorescence of S,N-CQDs and the prepared sensor has good selectivity for determining L-DOPA.

Smartphone-Based Fluorimeter Device for Rapid Determination of L-DOPA. BC was utilized as a substrate for preparing fluorescent carbon dot tape (S,N-CQDs-BC). The FE-SEM images of BC (Figure 7a) and S,N-CQDs-BC (Figure 7b) show that S,N-CQDs are entirely imprinted on the BC. Figure 7c shows the S,N-CQDs-BC under the 365 nm UV light captured by a smartphone device (Figure 7d) at different concentrations of L-DOPA. Under optimum conditions, PL emissive of S,N-CQDs-BC in the span of 1−250 μM was quenched by the interaction of L-DOPA and S,N-CQDs-BC. The intensity of S,N-CQDs-BC was measured by the RGB Color Detector app and the pictures were captured by the iPhone 6 camera. The linear response of the S,N-CQDs-BC (Figure 7e) was drawn (1−250 μM) and the LOD of 31.05 μM was calculated. Due to the changing of some conditions,

https://doi.org/10.1021/acsomega.3c01795
ACS Omega 2023, 8, 20987−20999

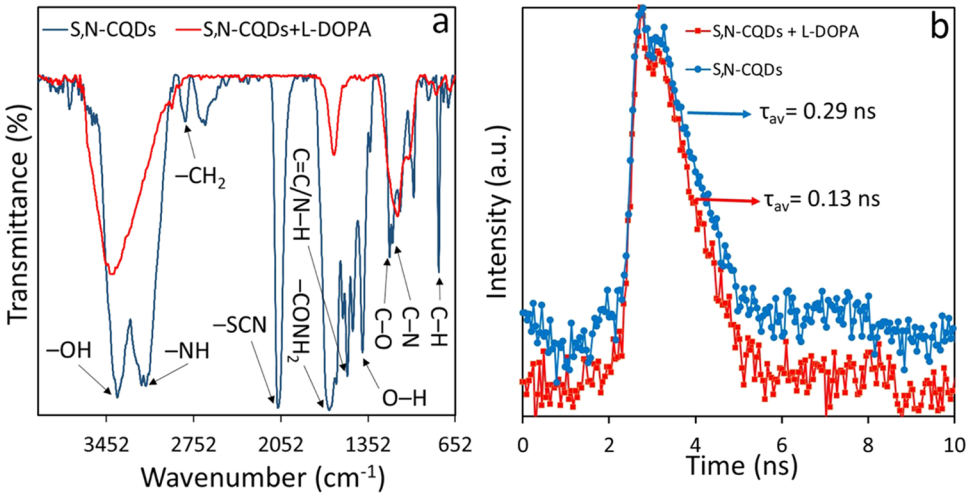

Figure 8. (a) FT-IR and (b) fluorescence lifetime decay of S,N-CQDs in the absence and presence of L-DOPA.

like the nature of substrates, it is predicted that the response of solid and liquid-based S,N-CQD sensors can be different.[46,80]

Mechanism of L-DOPA Determination. L-DOPA is an amino acid and dopamine, epinephrine, and norepinephrine are members of the catecholamine family, which can oxidize into quinone in alkaline environments. In alkaline solutions and the presence of oxygen, L-DOPA is oxidized to dopaquinone. Electron transfer interactions between CQDs and quinone occur during the oxidation of these materials like L-DOPA. S,N-CQDs and dopaquinone (electron acceptors) can interact, and the fluorescence of S,N-CQDs is quenched due to this reaction. This reaction changes the recombination kinetics of the electron and hole of photoexcited S,N-CQDs.[41] S,N-CQDs have some functional groups like hydroxyl and carboxyl groups, which can react with diols, amine groups, and phenyls in L-DOPA through electrostatic connections, $\pi-\pi$ stacking, and hydrogen bonding. Thiocyanate and other functional groups are electron-rich, and dopaquinone lacks electrons. Furthermore, nucleophilic functional groups can form covalent bonds with electrophilic dopaquinone (Scheme 2).[81] Also, the FT-IR spectra of S,N-CQDs (Figure 8a) and S,N-CQDs + L-DOPA confirmed that some functional groups like −SCN and $-NH_2$ interacted with L-DOPA due to the full disappearance of the −SCN and $-NH_2$ peaks. Finally, L-DOPA is oxidized to dopaquinone in alkaline solutions, which accept electrons from the S,N-CQDs, resulting in the quenching of fluorescence intensity.[82,83]

Fluorescence lifetime decay analysis was applied to investigate the quenching mechanism of S,N-CQDs (Figure 8b). Average fluorescence lifetime decay was calculated by eq S1 and the collected data are shown in Table S7. Due to the difference between the average fluorescence lifetime decay of the S,N-CQDs before and after the addition of L-DOPA, it can be concluded that the quenching mechanism involves dynamic quenching. This mechanism also results in photo-induced electron transfer between S,N-CQDs and dopaquinone, which causes fluorescence quenching of blue fluorescent S,N-CQDs.[41,84]

Determination of L-DOPA in Real Samples. The use of S,N-CQDs to determine L-DOPA in real samples such as human blood serum and urine was studied. 5, 10, and 25 μM of L-DOPA was added to human blood serum and urine samples in optimum conditions. The linear calibration of the prepared S,N-CQD sensor for the determination of L-DOPA was utilized in real sample application. Also, the regression equation was $y = 0.002x + 0.0025$ for real sample analysis. Table 1 displays the added L-DOPA and recovery results of

Table 1. Real Sample Recovery for L-DOPA Determination

sample	added L-DOPA (μM)	measured L-DOPA (μM)[a]	RSD (%)[b]	recovery (%)[c]
serum	5	5.23 ± 0.07	5.5	104.61
	25	24.71 ± 0.30	5.9	98.84
	50	49.21 ± 0.32	3.2	98.43
urine	5	4.86 ± 0.03	2.5	97.35
	25	25.92 ± 0.11	2.1	103.70
	50	52.15 ± 0.81	7.6	104.31

[a]Value = mean + standard deviation of three samples (n = 3). [b]Relative standard deviation = SD/mean × 100. [c]Recovery = measured value/added value × 100.

the L-DOPA determination in human blood serum and urine samples. From the calculation, the recoveries for human blood serum and urine samples were in the range of 98.4−104.6 and 97.3−104.3%, respectively. Also, the RSD range was 3.2−5.9 and 2.1−7.6% for human blood serum and urine samples, respectively. These outcomes show that the S,N-CQD sensor can determine L-DOPA with worthy selectivity and reproducibility in real samples. The results show that L-DOPA can be determined even in a complex environment with an acceptable selectivity. Also, the maximum plasma concentration of L-DOPA is in the range from 5 μM to 8 μM in the human body.[85] Therefore, the sensitivity of S,N-CQDs are suitable for the determination of L-DOPA in the human body.

CONCLUSIONS

Briefly, S,N-CQDs were synthesized for the first time by a green method using feijoa leaves as a precursor. S,N-CQDs exhibited strong blue fluorescence emission and good photostability for 30 days. The FT-IR of S,N-CQDs confirmed that the −SCN groups were introduced on S,N-CQDs which improved the interaction of L-DOPA with S,N-CQDs. Due to the interaction of S,N-CQDs with L-DOPA, the fluorescence emission of S,N-CQDs was quenched after the addition of various concentrations of L-DOPA. LOD of the S,N-CQDs in an aqueous solution was calculated at 0.45 μM. The

https://doi.org/10.1021/acsomega.3c01795
ACS Omega 2023, 8, 20987−20999

mechanism of quenching of the intensity of S,N-CQDs was investigated by FT-IR, and fluorescence lifetime decay spectroscopy. The PET process of dynamic quenching was confirmed as a sensing mechanism. Also, the smartphone-based fluorimeter device was designed to determine L-DOPA with S,N-CQDs-BC, which made it easier for analyte determination using any smartphone. Furthermore, the application of S,N-CQDs in real samples like human blood serum and urine was investigated, leading to the good recovery of 98.4−104.6 and 97.3−104.3% for human blood serum and urine samples, respectively, indicating the applicability of S,N-CQDs in complex environments.

■ ASSOCIATED CONTENT

Supporting Information

The Supporting Information is available free of charge at https://pubs.acs.org/doi/10.1021/acsomega.3c01795.

Optimization of conditions for the synthesis of S,N-CQDs, calculation of quantum yield data, calculation of lattice spacing from SAED analysis, ANOVA and Fit Statistics of the CCD model, calculation of τ_{av} for fluorescence lifetime decay, 3D model of the fluorimeter device, EDS spectra and elemental mapping of S,N-CQDs, Raman spectra of S,N-CQDs, adsorption−desorption isotherm and BET plot of the S,N-CQDs, absorption spectra of S,N-CQDs, S,N-CQDs + L-DOPA, and L-DOPA (PDF)

■ AUTHOR INFORMATION

Corresponding Author

Hamid Emadi − *Department of Applied Chemistry, Faculty of Chemistry, University of Mazandaran, Babolsar 4741695447, Iran;* orcid.org/0000-0002-2764-7264; Email: h.emadi@umz.ac.ir

Authors

Amir Hemmati − *Department of Applied Chemistry, Faculty of Chemistry, University of Mazandaran, Babolsar 4741695447, Iran*

Seyed Reza Nabavi − *Department of Applied Chemistry, Faculty of Chemistry, University of Mazandaran, Babolsar 4741695447, Iran;* orcid.org/0000-0002-2605-6710

Complete contact information is available at: https://pubs.acs.org/10.1021/acsomega.3c01795

Author Contributions

The manuscript was written through contributions of all authors. All authors have given approval to the final version of the manuscript.

Notes

The authors declare no competing financial interest.

■ ACKNOWLEDGMENTS

The authors thank the University of Mazandaran (UMZ) for financial support.

■ REFERENCES

(1) Hirsch, E. C.; Standaert, D. G. Ten unsolved questions about neuroinflammation in Parkinson's disease. *Mov. Disord.* **2021**, *36*, 16−24.

(2) Church, F. C. Treatment options for motor and non-motor symptoms of Parkinson's disease. *Biomolecules* **2021**, *11*, 612.

(3) Bjørklund, G.; Peana, M.; Maes, M.; Dadar, M.; Severin, B. The glutathione system in Parkinson's disease and its progression. *Neurosci. Biobehav. Rev.* **2021**, *120*, 470−478.

(4) Hornykiewicz, O. A brief history of levodopa. *J. Neurol.* **2010**, *257*, 249−252.

(5) Hauser, R. A. Levodopa: past, present, and future. *Eur. Neurol.* **2009**, *62*, 1−8.

(6) LeWitt, P. A. Levodopa for the treatment of Parkinson's disease. *N. Engl. J. Med.* **2008**, *358*, 2468−2481.

(7) Baião, V.; Tomé, L. I.; Brett, C. M. Iron oxide nanoparticle and multiwalled carbon nanotube modified glassy carbon electrodes. Application to levodopa detection. *Electroanalysis* **2018**, *30*, 1342−1348.

(8) Raghu, M.; Parashuram, L.; Kumar, K. Y.; Prasanna, B.; Rao, S.; Krishnaiah, P.; Prashanth, K.; Kumar, C. P.; Alrobei, H. Facile green synthesis of boroncarbonitride using orange peel; its application in high-performance supercapacitors and detection of levodopa in real samples. *Mater. Today Commun.* **2020**, *24*, No. 101033.

(9) Chen, C.; Zou, C.; Li, L.; Yu, H.; Zhu, J.; Liu, J.; Huang, W. Blue and green emission-transformed fluorescent copolymer: Specific detection of levodopa of anti-Parkinson drug in human serum. *Talanta* **2020**, *214*, No. 120817.

(10) Ghani, S. M.; Rezaei, B.; Jamei, H. R.; Ensafi, A. A. Novel synthesis of a dual fluorimetric sensor for the simultaneous analysis of levodopa and pyridoxine. *Anal. Bioanal. Chem.* **2021**, *413*, 377−387.

(11) Zhao, S.; Bai, W.; Wang, B.; He, M. Determination of levodopa by capillary electrophoresis with chemiluminescence detection. *Talanta* **2007**, *73*, 142−146.

(12) Sarre, S.; Michotte, Y.; Herregodts, P.; Deleu, D.; De Klippel, N.; Ebinger, G. High-performance liquid chromatography with electrochemical detection for the determination of levodopa, catecholamines and their metabolites in rat brain dialysates. *J. Chromatogr. B: Biomed. Sci. Appl.* **1992**, *575*, 207−212.

(13) Hormozi Nezhad, M. R.; Tashkhourian, J.; Khodaveisi, J. Sensitive spectrophotometric detection of dopamine, levodopa and adrenaline using surface plasmon resonance band of silver nanoparticles. *J. Iran. Chem. Soc.* **2010**, *7*, S83−S91.

(14) Zare, H.; Ghalkhani, M.; Akhavan, O.; Taghavinia, N.; Marandi, M. Highly sensitive selective sensing of nickel ions using repeatable fluorescence quenching-emerging of the CdTe quantum dots. *Mater. Res. Bull.* **2017**, *95*, 532−538.

(15) Khedkar, C.; Kalyankar, S.; Deosarkar, S. *Encyclopedia of Food and Health*; Academic Press: Oxford, 2016; Vol. *1*, pp 552−558.

(16) Zhu, S.; Ma, L.; Wang, S.; Chen, C.; Zhang, W.; Yang, L.; Hang, W.; Nolan, J. P.; Wu, L.; Yan, X. Light-scattering detection below the level of single fluorescent molecules for high-resolution characterization of functional nanoparticles. *ACS Nano* **2014**, *8*, 10998−11006.

(17) Magdy, G.; Hakiem, A. F. A.; Belal, F.; Abdel-Megied, A. M. Green one-pot synthesis of nitrogen and sulfur co-doped carbon quantum dots as new fluorescent nanosensors for determination of salinomycin and maduramicin in food samples. *Food Chem.* **2021**, *343*, No. 128539.

(18) Yao, J.; Yang, M.; Duan, Y. Chemistry, biology, and medicine of fluorescent nanomaterials and related systems: new insights into biosensing, bioimaging, genomics, diagnostics, and therapy. *Chem. Rev.* **2014**, *114*, 6130−6178.

(19) Magdy, G.; Said, N.; El-Domany, R. A.; Belal, F. Nitrogen and sulfur-doped carbon quantum dots as fluorescent nanoprobes for spectrofluorimetric determination of olanzapine and diazepam in biological fluids and dosage forms: application to content uniformity testing. *BMC Chem.* **2022**, *16*, No. 98.

(20) Yang, X.; Zhuo, Y.; Zhu, S.; Luo, Y.; Feng, Y.; Dou, Y. Novel and green synthesis of high-fluorescent carbon dots originated from honey for sensing and imaging. *Biosens. Bioelectron.* **2014**, *60*, 292−298.

(21) Alossaimi, M. A.; Elmansi, H.; Alajaji, M.; Altharawi, A.; Altamimi, A. S.; Magdy, G. A novel quantum dots-based fluorescent

sensor for determination of the anticancer dacomitinib: Application to dosage forms. *Molecules* **2023**, *28*, 2351.
(22) Baragau, I.-A.; Power, N. P.; Morgan, D. J.; Lobo, R. A.; Roberts, C. S.; Titirici, M.-M.; Middelkoop, V.; Diaz, A.; Dunn, S.; Kellici, S. Efficient continuous hydrothermal flow synthesis of carbon quantum dots from a targeted biomass precursor for on−off metal ions nanosensing. *ACS Sustainable Chem. Eng.* **2021**, *9*, 2559−2569.
(23) Akhavan, O.; Ghaderi, E. Graphene nanomesh promises extremely efficient in vivo photothermal therapy. *Small* **2013**, *9*, 3593−3601.
(24) Sedrpoushan, A.; Heidari, M.; Akhavan, O. Nanoscale graphene oxide sheets as highly efficient carbocatalysts in green oxidation of benzylic alcohols and aromatic aldehydes. *Chin. J. Catal.* **2017**, *38*, 745−757.
(25) Yuan, T.; Meng, T.; He, P.; Shi, Y.; Li, Y.; Li, X.; Fan, L.; Yang, S. Carbon quantum dots: an emerging material for optoelectronic applications. *J. Mater. Chem. C* **2019**, *7*, 6820−6835.
(26) Akhavan, O.; Bijanzad, K.; Mirsepah, A. Synthesis of graphene from natural and industrial carbonaceous wastes. *RSC Adv.* **2014**, *4*, 20441−20448.
(27) Magdy, G.; Elmansi, H.; Belal, F.; El-Deen, A. K. Doped carbon dots as promising fluorescent nanosensors: Synthesis, characterization, and recent applications. *Curr. Pharm. Des.* **2023**, *29*, 415−444.
(28) Weston, R. J. Bioactive products from fruit of the feijoa (Feijoa sellowiana, Myrtaceae): A review. *Food Chem.* **2010**, *121*, 923−926.
(29) MA, E.; Hosseinimehr, S.; Hamidinia, A.; Jafari, M. Antioxidant and free radical scavenging activity of Feijoa sellowiana fruits peel and leaves. *Pharmacologyonline* **2008**, *1*, 7−14.
(30) Su, R.; Wang, D.; Liu, M.; Yan, J.; Wang, J.-X.; Zhan, Q.; Pu, Y.; Foster, N. R.; Chen, J.-F. Subgram-scale synthesis of biomass waste-derived fluorescent carbon dots in subcritical water for bioimaging, sensing, and solid-state patterning. *ACS Omega* **2018**, *3*, 13211−13218.
(31) Tayyebi, A.; Akhavan, O.; Lee, B.-K.; Outokesh, M. Supercritical water in top-down formation of tunable-sized graphene quantum dots applicable in effective photothermal treatments of tissues. *Carbon* **2018**, *130*, 267−272.
(32) Magdy, G.; Belal, F.; Elmansi, H. Rapid microwave-assisted synthesis of nitrogen-doped carbon quantum dots as fluorescent nanosensors for the spectrofluorimetric determination of palbociclib: Application for cellular imaging and selective probing in living cancer cells. *RSC Adv.* **2023**, *13*, 4156−4167.
(33) Liu, M. L.; Chen, B. B.; Li, C. M.; Huang, C. Z. Carbon dots: synthesis, formation mechanism, fluorescence origin and sensing applications. *Green Chem.* **2019**, *21*, 449−471.
(34) de Medeiros, T. V.; Manioudakis, J.; Noun, F.; Macairan, J.-R.; Victoria, F.; Naccache, R. Microwave-assisted synthesis of carbon dots and their applications. *J. Mater. Chem. C* **2019**, *7*, 7175−7195.
(35) Sun, J.; Wang, W.; Yue, Q. Review on microwave-matter interaction fundamentals and efficient microwave-associated heating strategies. *Materials* **2016**, *9*, 231.
(36) Xu, Q.; Liu, Y.; Gao, C.; Wei, J.; Zhou, H.; Chen, Y.; Dong, C.; Sreeprasad, T. S.; Li, N.; Xia, Z. Synthesis, mechanistic investigation, and application of photoluminescent sulfur and nitrogen co-doped carbon dots. *J. Mater. Chem. C* **2015**, *3*, 9885−9893.
(37) Magdy, G.; Al-Enna, A. A.; Belal, F.; El-Domany, R. A.; Abdel-Megied, A. M. Application of sulfur and nitrogen doped carbon quantum dots as sensitive fluorescent nanosensors for the determination of saxagliptin and gliclazide. *R. Soc. Open Sci.* **2022**, *9*, No. 220285.
(38) Qin, Z.; Wang, W.; Zhan, X.; Du, X.; Zhang, Q.; Zhang, R.; Li, K.; Li, J.; Xu, W. One-pot synthesis of dual carbon dots using only an N and S co-existed dopant for fluorescence detection of Ag^{+}. *Spectrochim. Acta, Part A* **2019**, *208*, 162−171.
(39) Magdy, G.; Ebrahim, S.; Belal, F.; El-Domany, R. A.; Abdel-Megied, A. M. Sulfur and nitrogen co-doped carbon quantum dots as fluorescent probes for the determination of some pharmaceutically-important nitro compounds. *Sci. Rep.* **2023**, *13*, No. 5502.
(40) Park, S. W.; Kim, T. E.; Jung, Y. K. Glutathione-decorated fluorescent carbon quantum dots for sensitive and selective detection of levodopa. *Anal. Chim. Acta* **2021**, *1165*, No. 338513.
(41) Wang, C.; Shi, H.; Yang, M.; Yao, Z.; Zhang, B.; Liu, E.; Hu, X.; Xue, W.; Fan, J. Biocompatible sulfur nitrogen co-doped carbon quantum dots for highly sensitive and selective detection of dopamine. *Colloids Surf., B* **2021**, *205*, No. 111874.
(42) Amjadi, M.; Manzoori, J. L.; Hallaj, T.; Azizi, N. Sulfur and nitrogen co-doped carbon quantum dots as the chemiluminescence probe for detection of Cu^{2+} ions. *J. Lumin.* **2017**, *182*, 246−251.
(43) Banik, S.; Melanthota, S. K.; Arbaaz; Vaz, J. M.; Kadambalithaya, V. M.; Hussain, I.; Dutta, S.; Mazumder, N. Recent trends in smartphone-based detection for biomedical applications: a review. *Anal. Bioanal.Chem.* **2021**, *413*, 2389−2406.
(44) Golmohammadi, H.; Hamzei, Z.; Hosseinifard, M.; Ahmadi, S. H. Smart fully integrated lab: A Smartphone-Based compact miniaturized Analytical/Diagnostic device. *Adv. Mater. Technol.* **2020**, *5*, No. 2000742.
(45) Faham, S.; Golmohammadi, H.; Ghavami, R.; Khayatian, G. A nanocellulose-based colorimetric assay kit for smartphone sensing of iron and iron-chelating deferoxamine drug in biofluids. *Anal. Chim. Acta* **2019**, *1087*, 104−112.
(46) Morales-Narváez, E.; Golmohammadi, H.; Naghdi, T.; Yousefi, H.; Kostiv, U.; Horák, D.; Pourreza, N.; Merkoçi, A. Nanopaper as an optical sensing platform. *ACS Nano* **2015**, *9*, 7296−7305.
(47) Ugrinic, M.; Decanini, D.; Bidan, N.; Lazzari, G.; Harouri, A.; Hwang, G.; Haghiri-Gosnet, A.-M.; Mura, S. Fabrication of high aspect ratio microfluidic devices for long term in vitro culture of 3D tumor models. *Microelectron. Eng.* **2023**, *267*−*268*, No. 111898.
(48) Tabatabaee, R. S.; Golmohammadi, H.; Ahmadi, S. H. Easy diagnosis of jaundice: a smartphone-based nanosensor bioplatform using photoluminescent bacterial nanopaper for point-of-care diagnosis of hyperbilirubinemia. *ACS Sens.* **2019**, *4*, 1063−1071.
(49) Abbasi-Moayed, S.; Golmohammadi, H.; Hormozi-Nezhad, M. R. A nanopaper-based artificial tongue: a ratiometric fluorescent sensor array on bacterial nanocellulose for chemical discrimination applications. *Nanoscale* **2018**, *10*, 2492−2502.
(50) An, J.; Shi, Y.; Fang, J.; Hu, Y.; Liu, Y. Multichannel ratiometric fluorescence sensor arrays for rapid visual monitoring of epinephrine, norepinephrine, and levodopa. *Chem. Eng. J.* **2021**, *425*, No. 130595.
(51) Bandi, R.; Dadigala, R.; Gangapuram, B. R.; Guttena, V. Green synthesis of highly fluorescent nitrogen−doped carbon dots from Lantana camara berries for effective detection of lead (II) and bioimaging. *J. Photochem. Photobiol., B* **2018**, *178*, 330−338.
(52) Miao, X.; Yan, X.; Qu, D.; Li, D.; Tao, F. F.; Sun, Z. Red emissive sulfur, nitrogen codoped carbon dots and their application in ion detection and theraonostics. *ACS Appl. Mater. Interfaces* **2017**, *9*, 18549−18556.
(53) Koç, Ö. K.; Üzer, A.; Apak, R. High Quantum Yield Nitrogen-Doped Carbon Quantum Dot-Based Fluorescent Probes for Selective Sensing of 2, 4, 6-Trinitrotoluene. *ACS Appl. Nano Mater.* **2022**, *5*, 5868−5881.
(54) Raveendran, V.; Kizhakayil, R. N. Fluorescent carbon dots as biosensor, green reductant, and biomarker. *ACS Omega* **2021**, *6*, 23475−23484.
(55) Zhao, C.; Jiao, Y.; Hua, J.; Yang, J.; Yang, Y. Hydrothermal synthesis of nitrogen-doped carbon quantum dots as fluorescent probes for the detection of dopamine. *J. Fluoresc.* **2018**, *28*, 269−276.
(56) Zhang, X.; Zeng, Q.; Xiong, Y.; Ji, T.; Wang, C.; Shen, X.; Lu, M.; Wang, H.; Wen, S.; Zhang, Y.; et al. Energy level modification with carbon dot interlayers enables efficient perovskite solar cells and quantum dot based light-emitting diodes. *Adv. Funct. Mater.* **2020**, *30*, No. 1910530.
(57) Hou, X.; Li, Y.; Zhao, C. Microwave-assisted synthesis of nitrogen-doped multi-layer graphene quantum dots with oxygen-rich functional groups. *Aust. J. Chem.* **2016**, *69*, 357−360.
(58) Reckmeier, C.; Schneider, J.; Susha, A.; Rogach, A. Luminescent colloidal carbon dots: optical properties and effects of doping. *Opt. Express* **2016**, *24*, A312−A340.

https://doi.org/10.1021/acsomega.3c01795
ACS Omega 2023, 8, 20987−20999

(59) Markgraf, S. A.; Reader, J. R. Calculated from ICSD using POWD-12++,(1997). *Mineral* **1985**, *70*, 590.
(60) Wei, X.-M.; Xu, Y.; Li, Y.-H.; Yin, X.-B.; He, X.-W. Ultrafast synthesis of nitrogen-doped carbon dots via neutralization heat for bioimaging and sensing applications. *RSC Adv.* **2014**, *4*, 44504−44508.
(61) Jones, S. S.; Sahatiya, P.; Badhulika, S. One step, high yield synthesis of amphiphilic carbon quantum dots derived from chia seeds: a solvatochromic study. *New J. Chem.* **2017**, *41*, 13130−13139.
(62) Sangam, S.; Gupta, A.; Shakeel, A.; Bhattacharya, R.; Sharma, A. K.; Suhag, D.; Chakrabarti, S.; Garg, S. K.; Chattopadhyay, S.; Basu, B.; et al. Sustainable synthesis of single crystalline sulphur-doped graphene quantum dots for bioimaging and beyond. *Green Chem.* **2018**, *20*, 4245−4259.
(63) Kumar, M.; Tomar, M.; Amarowicz, R.; Saurabh, V.; Nair, M. S.; Maheshwari, C.; Sasi, M.; Prajapati, U.; Hasan, M.; Singh, S.; et al. Guava (*Psidium guajava* L.) leaves: Nutritional composition, phytochemical profile, and health-promoting bioactivities. *Foods* **2021**, *10*, 752.
(64) Tanpure, S.; Ghanwat, V.; Shinde, B.; Tanpure, K.; Lawande, S. The eggshell waste transformed green and efficient synthesis of K-Ca (OH) 2 catalyst for room temperature synthesis of chalcones. *Polycyclic Aromat. Compd.* **2022**, *42*, 1322−1340.
(65) Zaman, A. S. K.; Tan, T. L.; et al. Properties and molecular structure of carbon quantum dots derived from empty fruit bunch biochar using a facile microwave-assisted method for the detection of Cu^{2+} ions. *Opt. Mater.* **2021**, *112*, No. 110801.
(66) Tian, X. T.; Yin, X. B. Carbon dots, unconventional preparation strategies, and applications beyond photoluminescence. *Small* **2019**, *15*, No. 1901803.
(67) Yoo, D.; Park, Y.; Cheon, B.; Park, M.-H. Carbon dots as an effective fluorescent sensing platform for metal ion detection. *Nanoscale Res. Lett.* **2019**, *14*, 1−13.
(68) Luo, H.; Lari, L.; Kim, H.; Hérou, S.; Tanase, L. C.; Lazarov, V. K.; Titirici, M.-M. Structural evolution of carbon dots during low temperature pyrolysis. *Nanoscale* **2022**, *14*, 910−918.
(69) Nespolo, M. Numerical Problems in Crystallography. By MA Wahab. Springer, 2021. Hardcover, pp. xv+ 387. ISBN 9789811597534. Price EUR 83.19. *Acta Crystallographica Section A: Foundations and Advances* **2022**, *78*, 59−62.
(70) He, M.; Zhang, J.; Wang, H.; Kong, Y.; Xiao, Y.; Xu, W. Material and optical properties of fluorescent carbon quantum dots fabricated from lemon juice via hydrothermal reaction. *Nanoscale Res. Lett.* **2018**, *13*, No. 175.
(71) Yeh, T.-F.; Chen, S.-J.; Teng, H. Synergistic effect of oxygen and nitrogen functionalities for graphene-based quantum dots used in photocatalytic H_2 production from water decomposition. *Nano Energy* **2015**, *12*, 476−485.
(72) Kumari, M.; Chaudhary, G. R.; Chaudhary, S.; Umar, A.; Akbar, S.; Baskoutas, S. Bio-Derived Fluorescent Carbon Dots: Synthesis, Properties and Applications. *Molecules* **2022**, *27*, 5329.
(73) Bhatt, M.; Bhatt, S.; Vyas, G.; Raval, I. H.; Haldar, S.; Paul, P. Water-dispersible fluorescent carbon dots as bioimaging agents and probes for Hg^{2+} and Cu^{2+} ions. *ACS Appl. Nano Mater.* **2020**, *3*, 7096−7104.
(74) Qin, X.; Lu, W.; Asiri, A. M.; Al-Youbi, A. O.; Sun, X. Microwave-assisted rapid green synthesis of photoluminescent carbon nanodots from flour and their applications for sensitive and selective detection of mercury (II) ions. *Sens. Actuators, B* **2013**, *184*, 156−162.
(75) Eaton, D. F. Reference materials for fluorescence measurement. *Pure Appl. Chem.* **1988**, *60*, 1107−1114.
(76) Würth, C.; Grabolle, M.; Pauli, J.; Spieles, M.; Resch-Genger, U. Relative and absolute determination of fluorescence quantum yields of transparent samples. *Nat. Protoc.* **2013**, *8*, 1535−1550.
(77) Moslehipour, A.; Bigdeli, A.; Ghasemi, F.; Hormozi-Nezhad, M. R. Design of a ratiometric fluorescence nanoprobe to detect plasma levels of levodopa. *Microchem. J.* **2019**, *148*, 591−596.
(78) Issa, M. A.; Abidin, Z. Z.; Sobri, S.; Rashid, S. A.; Mahdi, M. A.; Ibrahim, N. A. Fluorescent recognition of Fe^{3+} in acidic environment by enhanced-quantum yield N-doped carbon dots: Optimization of variables using central composite design. *Sci. Rep.* **2020**, *10*, No. 11710.
(79) Hu, M.; Yu, H.; Wei, F.; Xu, G.; Yang, J.; Cai, Z.; Hu, Q. Citrate-capped Mn-modified CdSe/CdS quantum dots as luminescent probes for levodopa detection in aqueous solution. *Spectrochim. Acta, Part A* **2012**, *91*, 130−135.
(80) Álvarez-Diduk, R.; Orozco, J.; Merkoçi, A. Paper strip-embedded graphene quantum dots: a screening device with a smartphone readout. *Sci. Rep.* **2017**, *7*, No. 976.
(81) Liu, J.-J.; Zhang, X.-L.; Cong, Z.-X.; Chen, Z.-T.; Yang, H.-H.; Chen, G.-N. Glutathione-functionalized graphene quantum dots as selective fluorescent probes for phosphate-containing metabolites. *Nanoscale* **2013**, *5*, 1810−1815.
(82) Byszewska, W.; Kańska, M. Studies on enzymatic oxidation of 3′, 4′-dihydroxy-l-phenylalanine to dopachrome using kinetic isotope effect methods. *J. Radioanal. Nucl. Chem.* **2014**, *299*, 1373−1378.
(83) Waite, J. H. Mussel adhesion−essential footwork. *J. Exp. Biol.* **2017**, *220*, 517−530.
(84) Wang, C.; Shi, H.; Yang, M.; Yan, Y.; Liu, E.; Ji, Z.; Fan, J. A novel nitrogen-doped carbon quantum dots as effective fluorescent probes for detecting dopamine. *J. Photochem. Photobiol., A* **2020**, *391*, No. 112374.
(85) Iwaki, H.; Nishikawa, N.; Nagai, M.; Tsujii, T.; Yabe, H.; Kubo, M.; Ieiri, I.; Nomoto, M. Pharmacokinetics of levodopa/benserazide versus levodopa/carbidopa in healthy subjects and patients with P arkinson's disease. *Neurol. Clin. Neurosci.* **2015**, *3*, 68−73.

https://doi.org/10.1021/acsomega.3c01795
ACS Omega 2023, 8, 20987−20999